*International Journal of Power and Energy Systems, Vol. 46, No. 10, 2026*
*An Open Access Paper*

# FULL-TIME-DOMAIN POWER EQUALIZATION COOPERATIVE CONTROL OF MMC-BESS WITH STRING SWARM ARCHITECTURE BASED ON SENSOR MULTIPARAMETER ESTIMATION

Zhuohang Chen,* Tao Bo,** Ruixiong Yang,* and Jianduo Li**

**Abstract**

The Modular Multi-Level Battery Energy Storage System (MMC-BESS) is an energy storage system based on modular multi-level converter technology. Its core component is a battery bank, which achieves efficient energy conversion and energy storage scheduling by distributing a large number of battery cells across various power submodules for decentralized management. To ensure that the MMC-BESS cascade architecture maintains power balance distribution throughout the entire time domain and adapts to multi scenario requirements, this paper proposes a collaborative control method for full time domain power balance based on sensor multi parameter estimation. This method innovatively uses passive non-contact current sensors and inverse piezoelectric grating voltage sensing units to achieve high-precision full time domain acquisition of AC/DC voltage/current. Based on multi parameter estimation, the electrical parameters of the upper and lower bridge arms of each phase cluster are obtained to achieve DC side power balance control and bridge arm submodule AC/DC power regulation. Finally, the full time domain power balance of the system is maintained through submodule charge state balance. The experimental results show that the maximum SOC difference of the submodule after control is only 0.12, and the percentage of capacitor voltage fluctuation is less than 5%. Compared with traditional methods, the power balance accuracy is improved by 65%, which verifies the effectiveness of the method in full time domain dynamic response and steady-state stability.

* Zhuhai Power Supply Bureau, Guangdong Power Grid Co., Ltd., Zhuhai, 519000, China; e-mail: tanteng14122248346@163.com; chekuang6349377290@163.com
** Global Mainstream Dynamic Energy Technology Ltd., Hangzhou, 310000, China; e-mail: zibitan124@163.com; luweizhuolu6@163.com
Corresponding author: Tao Bo

*Recommended by: Saeed Rezaeian-Marjani*
*(DOI:10.2316/J.2026.203-0617)*

**Key Words**

Sensors; Multiparameter estimation; Crosstalk architecture; MMC-BESS; Full-Time domain; Power equalization; Cooperative control

## 1. Introduction

String cluster architecture is a type of energy storage system structure that combines multiple battery modules in series and parallel to improve the flexibility and scalability of the energy storage system, increase the energy storage capacity and power output ability of the system [1], and modularize the system according to the actual needs of the increase or decrease [2], in order to adapt to different application scenarios and needs. At the same time, the string group architecture also helps to realize the balanced control between the battery packs to improve the performance and stability of the whole energy storage system. MMC-BESS is a battery energy storage system based on MMC technology, the core of which is the battery pack [3], which plays the role of storing and releasing energy in the energy storage system [4]. Based on this, the string cluster architecture of MMC-BESS is characterized by modularity and scalability, in which multiple battery modules are combined in series and parallel to form an overall energy storage system [5], which can improve the flexibility and reliability of BESS. Owing to the differences in the performance and state of each energy storage module in the string cluster architecture MMC-BESS, power equalization control is required to ensure the stable operation of the system, among which power balance refers to the whole system's power distribution by adjusting the power output between multiple systems or components. Collaborative control can ensure the power output of each component, ensure the long life and high performance of the battery pack, and achieve optimal energy utilization and

power grid stability. To address the power imbalance issues caused by module performance differences in the full-time domain operation of the MMC-BESS series-connected architecture, and to enhance system stability and energy utilization efficiency, it is necessary to conduct research on this topic.

Zhang et al. [6] proposed a power fluctuation control method for a supercapacitor hybrid energy storage system. A mathematical model of the battery state of charge (SOC) was established to analyze the charging and discharging power and SOC status of the energy storage device in the hybrid energy storage system. A low-pass filtering method was used to determine the power reference value of the energy storage device in the system, and a fuzzy neural PID controller was designed to achieve power fluctuation control of the hybrid energy storage system based on the power reference values of the supercapacitor and battery. However, the performance of fuzzy neural PID controllers is highly dependent on their parameter settings and training data. If the parameters are set incorrectly or the training data is insufficient, the controller may perform poorly and be unable to effectively control power fluctuations. Rasool et al. [7] propose an effective power control strategy based on dynamic filter power distribution, considering the operational characteristics of a hybrid energy storage system. This strategy allocates low-frequency and high-frequency power components to optimize the efficiency and response speed of energy storage equipment utilization. The approach aims to achieve real-time control of hybrid energy storage systems, ensuring stable power output under various conditions to meet the requirements of power grids or loads. However, the dynamic filter primarily relies on frequency characteristics, whereas the power requirements of hybrid energy storage systems may involve multiple frequency components and dynamic changes. Consequently, the filtering strategy may not fully address the system's needs. Jeon et al [8] proposed a joint optimization framework to ensure effective scheduling of the energy storage system. This framework integrates the operation of voltage regulators (e.g., load tap changers, capacitor banks, and smart inverters of photovoltaic systems) with the path planning of the mobile energy storage system. The primary objectives are to minimize actual power loss and voltage deviation while achieving peak shaving and valley filling, thereby optimizing power control. During implementation, the stability and robustness of the joint optimization framework may be affected by disturbances such as load fluctuations and equipment failures. Ebrahimi et al [9], in order to ensure the control effect of the energy storage system, according to the characteristics of the energy storage system, the load demand of the power grid and the results of state prediction, develop a set of optimal charging and discharging plan, dynamically adjust the charging and discharging strategy of the energy storage system, so that the energy storage system can be reasonably allocated in different time periods of charging and discharging power to meet the demand of the grid and maximize its energy storage efficiency. Maximizing its energy storage efficiency to ensure that the energy storage system can always be maintained in the optimal state of operation, the algorithm in the process of operation of the method depends on the prediction of the future situation. If the prediction results of the deviation it will directly affect the control results, especially in large-scale energy storage systems, it is impossible to guarantee the control effect. Hanif et al [10] considered the objectives of maximizing economic benefits, minimizing power loss, maintaining grid stability, and dynamically adjusting the charging and discharging power according to real-time grid demand, renewable energy generation, and the current state of the BESS to ensure that the BESS can provide the optimal service in different time periods. In the process of practical application, if the state of the BESS changes and the demand of the grid increases, the control of the algorithm will decrease in real time and cannot guarantee the control effect. Mendi et al. [11]proposed a maximum power point tracking method based on a single load current sensor with adaptive step length. This method utilizes load current information to track maximum power without requiring rotor speed information or turbine parameter knowledge. A simple and cost-effective switch-mode rectifier topology is adopted for variable-speed WECS based on PMSG, which achieves higher tracking efficiency, faster tracking speed, and improved steady-state and transient performance. However, the load current information itself may be affected by various factors, such as load changes and grid fluctuations, which may interfere with accurate tracking of the maximum power point.

Sensor multiparameter estimation refers to the process of using sensor technology to simultaneously acquire multiple target parameters and calculate the parameters through analytical methods, which usually involves the use of multiple categories of sensors to sense target data and the analysis and calculation of the sensed data, so as to realize the estimation and analysis of physical or chemical quantities. Therefore, in the full-time power equalization control of the MMC-BESS of the cascade group architecture, the MMC-BESS can acquire multiple key electrical parameters, such as voltage, current, temperature, etc., which provide a reliable data basis for the subsequent power equalization control. Therefore, in this paper, a full-time power equalization and cooperative control method based on multi-parameter estimation of sensors is proposed for the MMC-BESS with swarm architecture, which combines multiple sensors to perceive the MMC-BESS data and utilizes the results of multi-parameter estimation of sensors to more accurately grasp the operating state of the BESS at different time scales to formulate a more reasonable control strategy and realize power equalization and cooperative control in the full-time domain.

Existing methods have shortcomings in addressing the coupling of module performance variability and full-time domain power fluctuations in string-based architectures, and they do not fully utilize multi-source sensor data, making it impossible to solve problems from a full-time domain multi-parameter fusion perspective. In contrast, the method proposed in this paper utilizes passive non-contact current sensors and inverse piezoelectric voltage sensing units to achieve full-time domain electrical data

acquisition. By constructing a bridge arm electrical model based on multi-parameter estimation, the method innovatively decouples the control of AC and DC power, reducing the maximum SOC difference among submodules by 66% under 30% load fluctuations, keeping capacitor voltage fluctuations within 4.26%, and shortening the dynamic response adjustment time by 58%. This addresses the challenge that traditional methods struggle to balance the dynamic changes of multiple parameters across the entire time domain with the coupling between modules in a stringed array architecture.

The main contributions of this paper are as follows:

(1) A full-time domain electrical data acquisition scheme based on multi-source sensors is proposed to achieve high-precision synchronous measurement of AC and DC parameters;
(2) A bridge arm electrical parameter estimation model for the series-parallel architecture is established to decouple AC and DC power control and design a submodule SOC balancing strategy;
(3) The post-control submodule SOC differences and capacitor voltage fluctuations are both superior to traditional PI control methods and do not rely on accurate predictions.

The organizational structure of this article is as follows: The introduction section introduces the basic concepts and characteristics of string group architecture and MMC-BESS, summarizes the shortcomings of existing related control strategies, and highlights the necessity of proposing the method in this article; Chapter 2 elaborates on the method of multi parameter estimation for sensors, conducts electrical parameter estimation for the MMC-BESS series group architecture, and constructs its topology and mathematical model; Chapter 3 validated the effectiveness of the proposed control method through testing and analysis; The conclusion section summarizes the research findings and contributions.

## 2. String Cluster Architecture MMC-BESS Full-Time Domain Power Equalization Cooperative Control

### 2.1 Sensor Multiparameter Estimation

#### *2.1.1 Multi-Source Sensor-based String Cluster Architecture MMC-BESS Operating Full-Time Domain Electrical Quantity Data Acquisition*

To ensure the full-time power equalization control effect of the MMC-BESS, reliable electrical data must be obtained in its full-time domain [12]. Therefore, combined with the operating and structural characteristics of the cluster architecture MMC-BESS, a multi-source sensor is used to collect the voltage and current in the entire operation time domain. The overall structure of the electrical data acquisition system based on the multi-source sensor is shown in Figure 1.

During the entire acquisition process, the current, voltage, and temperature data are mainly collected, in which

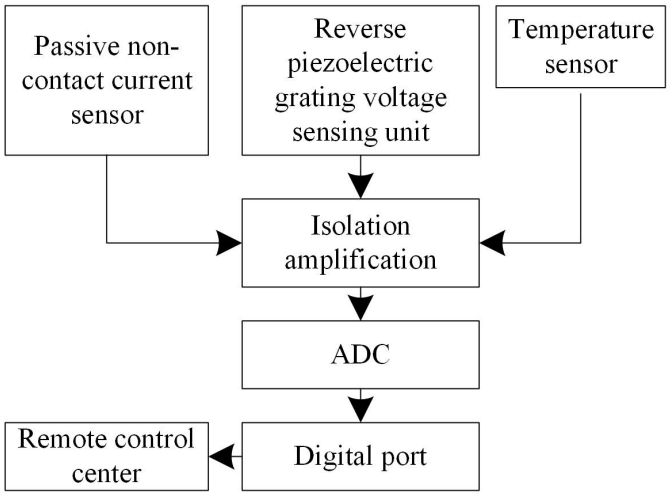


Figure 1. MMC-BESS Operating Full Time Domain Electrical Data Acquisition Structure Based on Multi-Source Sensor Cluster Architecture

the temperature data are directly obtained through the temperature sensor, the current and voltage data are collected through the passive non-contact current sensor and the inverse piezoelectric-grating voltage sensing unit, respectively [13], and the collected data are processed directly through the microcontroller. The data are transmitted to the external device through the digital port according to the data protocol, and the external device is connected to the remote control center through the external interface. The remote center stores the collected data, performs parameter estimation, and carries out the MMC-BESS full-time domain power equalization of the string group architecture.

#### *2.1.2 Current Data Acquisition Based on Passive Non-Contact Current Sensors*

Passive non-contact current sensors usually have a specific sensing structure design, which is based on the composition of super magnetostrictive material (GMM) and fiber optic grating (FBG), and can realize non-contact measurement of the current, which has the advantages of no need for direct contact with the current conductor, no additional resistance, and low measurement error. When the current in the MMC-BESS passes through the wire, a magnetic field is generated around the wire. This magnetic field is collected by the core of the sensor and induced in the coil or the sensitive element. The sensitive element detects a change in the magnetic field and converts it into an electrical signal output. These electrical signals are amplified and processed to accurately represent the current data of the MMC-BESS.

Passive non-contact current sensors generate axial magnetostatic strain $\varepsilon$ in the GMM during current data acquisition. the correlation between the strain and direction of the magnetic field $\psi$ is:

$$\varepsilon = C\psi^2 \tag{1}$$

Where: $C$ denotes the strain coefficient.

Equation (1) is an even function, which is simplified when it is in the linear operating interval to give:

$$\varepsilon = C\psi \tag{2}$$

In the grating part, the expansion and contraction of GMM under the influence of magnetic field induces axial expansion and contraction of the sensing FBG bonded to it, resulting in a shift of the center wavelength of the reflectance spectrum of the sensing FBG. Additionally, ambient temperature contributes to the shift of the center wavelength of the FBG. Under the combined effect of temperature and strain, the calculation formula for the shift of the center wavelength is as follows:

$$\frac{\Delta\lambda_o}{\lambda_o} = (1-\rho_e)\frac{\Delta L_o}{L_o} + (\kappa+\chi)\Delta T \tag{3}$$

Where: $\lambda_o$ and $\Delta\lambda_o$ are the FBG center wavelength and center wavelength offset, respectively; $L_o$ and $\Delta L_o$ are the FBG grid-area length and the grid-area length morphology variables, respectively; $\rho_e, \kappa$, and $\chi$ are the elasto-optical, thermal expansion, and thermo-optical coefficients of the FBG, respectively; $\Delta T$ indicates the amount of change in the external ambient temperature.

According to the working principle of the sensor, the deformation of the length of the FBG gate area is the deformation of the GMM transferred to the FBG by the optical glue under the action of the magnetic field $\Delta L$ , i.e $\Delta L \approx \Delta L_o$, the relationship between the wavelength variation of the sensor and the magnetic field to be measured in the linear operating interval can be determined by synthesizing Eqs. (1) and (2) as follows:

$$\frac{\Delta\lambda_o}{\lambda_o} = (1-\rho_e)\frac{C\psi L}{L_o} + (\kappa+\chi)\Delta T \tag{4}$$

Where: $L$ indicates the GMM length.

Equation (4) shows that the wavelength shift of the FBG center is linear with the input magnetic field and the temperature change, in which the temperature change has nothing to do with the input signal, and it is the environmental factor that affects the wavelength shift of the center of the FBG; Neglecting the influence of temperature. Equation (4) can be expressed as follows:

$$\frac{\Delta\lambda_o}{\psi} = (1-\rho_e)\frac{CL}{L_o} \tag{5}$$

Equation (5) can detect the changes in the magnetic field and convert it into an electrical signal output, which is processed and converted into an electrical signals output that can be used to represent the magnitude and direction of the current to obtain the current data of the string group architecture MMC-BESS [14].

#### *2.1.3 Voltage Data Acquisition Based on an Inverse Piezoelectric-Grating Voltage Sensing Unit*

The whole inverse piezoelectric - grating voltage sensing unit consists of piezoelectric ceramic FBG, copper electrode, wire and optical glue, which in the string group architecture MMC-BESS voltage data acquisition, the AC voltage signal to be measured through the wire and copper electrode added to the piezoelectric module at both ends, according to the inverse piezoelectric effect, when the direction of the voltage to be measured and the direction of polarization of the piezoelectric module is the same, piezoelectric modules will be along the direction of polarization of the stretch deformation. When the direction of the voltage to be measured changes and is opposite to the polarization direction of the piezoelectric module, the piezoelectric module in the direction of polarization will rapidly change from a tensile deformation to a contraction deformation; and through the optical glue and the piezoelectric module directly connected to the FBG will be subjected to the axial stress generated by the deformation of the piezoelectric module, resulting in the output spectral shift in the optical path, and ultimately through the detection of the center of the wavelength of the change in the amount of the inverse calculation of the crosstalk architecture. MMC-BESS voltage signal.

To ensure the effectiveness of this sensor for the collection of voltage data, the displacement transfer coefficient is introduced to obtain the relationship between the wavelength offset of the center of the FBG and the variation in the voltage and temperature to be measured, which is expressed as follows:

$$\Delta L = \varepsilon\Delta d \tag{6}$$

$$\Delta\widetilde{\lambda} = (1-\rho_e)\varepsilon n d_3 U\lambda_o + (\chi+\zeta)\Delta T\lambda_o \tag{7}$$

Where: $\Delta\widetilde{\lambda}$ denotes the amount of change in the center wavelength of the grating fiber after a change in the environmental parameters. $\varepsilon$ denotes the displacement transfer coefficient. $\Delta d$ denotes the total morphology of the gauge piezoelectric module along the polarization direction; $n$ denotes the number of stacks of piezoelectric ceramics in the piezoelectric module; $d_3$ denotes the piezoelectric constant; $U$ is the voltage applied externally to the piezoelectric ceramic surface.

The first term on the right-hand side of the equation represents the change in the center wavelength caused by the deformation of the grating owing to the voltage signal to be measured. Keeping the ambient temperature unchanged or eliminating the effect of temperature on the center wavelength, the following can be obtained:

$$\Delta\lambda = (1-\rho_e)\varepsilon n d_3 U\lambda_o \tag{8}$$

At this time, the output spectrum of the inverse piezoelectric grating voltage sensing unit contains only the information of the voltage to be measured, and the voltage of the crosstalk group architecture MMC-BESS can be back-calculated by demodulating the output spectrum with the demodulation equipment.

The voltage and current of the DC side and AC side of the string group architecture MMC-BESS are collected through the above two subsections, the acquired DC side voltage is indicated by the $v_e$, the AC side voltage and current are represented by $v_u$ and $i_u$ that the obtained current

and voltage results are used in the parameter estimation of the subsequent string cluster architecture MMC-BESS.

### 2.2 Electrical Quantity Parameter Estimation for the String Cluster Architecture MMC-BESS

The MMC-BESS consists of three-phase clusters, each of which is divided into upper and lower bridge arms, each of which contains N sub-modules (Sub-Module, SM). The sub-module consists of a half-bridge circuit, a battery, and a filter capacitor, where the battery is directly connected in parallel to the two ends of the filter capacitor. The topology of the MMC-BESS with a string cluster architecture is shown in Figure 2.

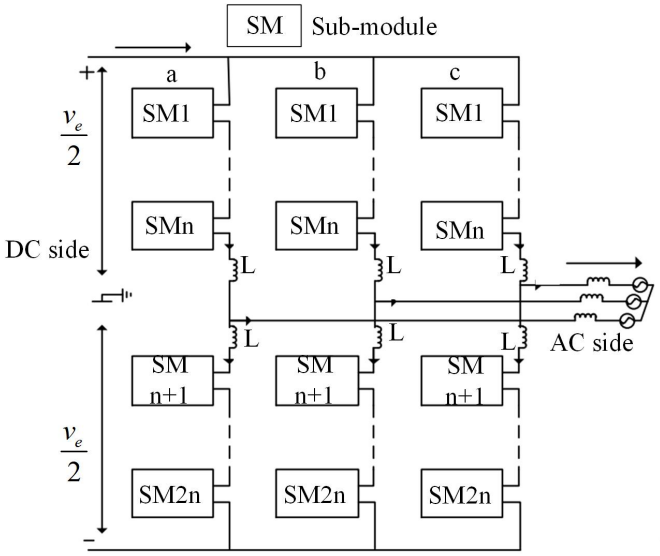


Figure 2. Cluster Architecture MMC-BESS Topology Structure

The string cluster architecture MMC-BESS structure in the upper and lower total of six bridge arm compositions, the upper and lower bridge arms through the bridge arm inductance $L$ connected to the concatenated network points, each consisting of $N$ single power sub-module, a single power sub-module consisting of a half-bridge sub-module, a connecting inductor $L_e$ and a battery; The voltage of each bridge arm in the structure is calculated according to the $v_e$ and $v_u$ collected in the above section, and the calculation formula is:

$$\begin{cases} \bar{v}_k = \dfrac{v_e}{2} - v_k^u \\ \vec{v}_k = \dfrac{v_e}{2} + v_k^u \end{cases} \tag{9}$$

Where: $\overleftarrow{v}_k$ is $k$-phase arm voltage; $\overrightarrow{v}_k$ is $k$-phase arm voltage; $v_k^u$ is $k$-phase AC side voltage, $k = a, b, c$ indicates a, b, and c phases.

The current of each bridge arm in the structure is calculated according to $i_u$ collected in the previous section, and the calculation formula is as follows:

$$\begin{cases} \overleftarrow{i}_k^u = -\dfrac{i_k^u}{2} + i_o^u \\ \overrightarrow{i}_k^u = \dfrac{i_k^u}{2} + i_o^u \end{cases} \tag{10}$$

Where: $\overleftarrow{i}_k^u$ is the $k$-phase up arm current; $\vec{i}_k^u$ is the $k$-phase down arm current; $i_k^u$ is the $k$-phase AC side current; $i_o^u$ is the $k^k$-phase MMC circulation.

Based on the above equation, the power of each bridge arm is calculated as follows:

$$\begin{cases} \overleftarrow{P}_k = -\dfrac{v_e}{2}\dfrac{i_k^u}{2} + \dfrac{v_e}{2} i_o^u + v_k^u \dfrac{\overleftarrow{i}_k^u}{2} - v_k^u i_o^u \\ \overrightarrow{P}_k = -\dfrac{v_e}{2}\dfrac{i_k^u}{2} + \dfrac{v_e}{2} i_o^u + v_k^u \dfrac{\overrightarrow{i}_k^u}{2} - v_k^u i_o^u \end{cases} \tag{11}$$

Where: $\overleftarrow{P}^k$ denotes $k$-phase upper bridge arm power. $\overrightarrow{P}^k$ denotes $k$-phase down bridge arm power.

Based on the theory of coordinate transformations convert $i_a^{lu} i_b^{lu} i_c^{lu}$ so that they form $\alpha, \beta$ axis currents, respectively represented by $i_\alpha, i_\beta$. Park's transformation is then applied to this current, and the MMC-BESS mathematical model of the cluster architecture in $dq$ coordinate system is obtained:

$$\begin{cases} L\dfrac{di_d}{dt} = u_d - u_d^g + \omega L i_q \\ L\dfrac{di_q}{dt} = u_q - u_q^g - \omega L i_d \end{cases} \tag{12}$$

In the formula, $u_d$ is the MMC-BESS $d$ axis voltage. $u_d^g$ is grid $d$ axis voltage. $u_q$ is system $q$ axis voltage. $u_q^g$ is grid $q_{\text{axis voltage.}}$ $L$ denotes the equivalent inductance. $i_d, i_q$ denote current of $d$ axis and $q$ axis.

### 2.3 Full-Time Domain Power Equalization Control for the String Cluster Architecture MMC-BESS

#### *2.3.1 Full-Time Domain Control of the String Cluster Architecture MMC-BESS*

The full-time domain power control of MMC-BESS with string group architecture constitutes a fundamental function of the battery energy storage system, and rapid, precise power response is a critical requirement imposed by the grid on MMC-BESS. Furthermore, additional advanced control strategies for MMC-BESS are implemented based on the power control function, rendering the establishment of the power control model essential for effective management of the battery energy storage system [15]. Given the presence of DC ports and AC ports in the string cluster architecture MMC-BESS, it is necessary to control DC power and AC power independently while achieving decoupling control between AC and DC power. The block diagram of the MMC-BESS power system with a string cluster architecture is shown in Figure 3.

(1) DC power control: The DC power of the system is the product of the system DC voltage and DC current. Because the system DC bus is directly connected to

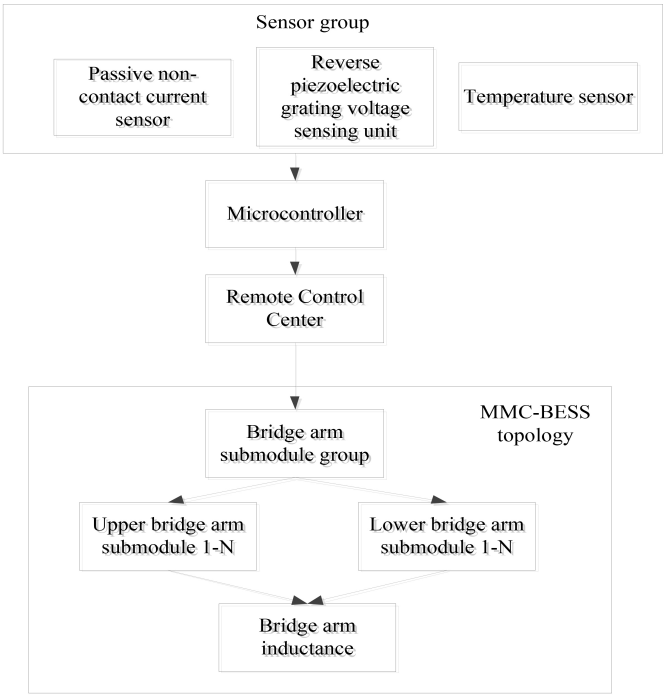


Figure 3. String Cluster Architecture MMC-BESS Power System Schematic Diagram

the DC grid, the DC bus voltage is fixed, and thus, the formula for the DC bus current $i_e$ is:

$$i_e = \frac{P_0}{v_e} \tag{13}$$

Where: $P_0$ indicates the given power on the DC side. According to Kirchhoff's current law, the sum of the three-phase DC currents of the system should be equal to the DC bus current [16], because the three-phase parameters of the system are the same in the ideal case, the given values of the DC currents of each phase should be equal, and the sum of the DC currents of each phase is equal to the DC bus current, then the formula for the DC given current $i_0^e$ is:

$$i_0^e = \frac{i_e}{3} \tag{14}$$

Combined with the characteristics of the string cluster architecture MMC-BESS, the DC current is controlled using PI regulation, and the DC-side control is controlled as follows:

$$v_0^e = -\left[(i_0^e - i_k^u)\left(\xi_p + \frac{\xi_I}{s}\right) - v_e\right] \tag{15}$$

Where: $v_0^e$ is the given value of the system DC voltage. $\xi_p$ is a DC current loop pparameters; $\xi_I$ is a DC current loop $I$ parameters.

(2) AC power control: According to the definition of a synchronized rotating coordinate system, the $d$ axis can be calibrated to the AC grid voltage phasor. Thus, the AC grid voltage and system AC current phasor can be decomposed into the coordinate system of $dq$ axis.

$$\begin{cases} \widehat{v}_g = u_d^g + ju_q^g \\ \widehat{i} = i_d + ji_q \end{cases} \tag{16}$$

Where: $\widehat{v}_g$ denotes the phase of the AC grid voltage. $\widehat{i}$ indicates the system AC current phase.

According to the power law of a symmetrical three-phase AC system, the complex power of the AC grid is the dot product of the AC grid voltage phase and AC current phase, which is calculated as follows:

$$\begin{cases} P_\Sigma = \frac{3}{2}\widehat{v}_g\hat{i} \\ P_\Sigma = P + jQ \end{cases} \tag{17}$$

Where: $P_\Sigma$ denotes the output complex power of the AC side of the system; $P$ is the active power on the AC side; $Q$ indicates the reactive power on the AC side. Combining Eq. (16) and Eq. (17) above yields:

$$\begin{cases} \frac{2}{3}P = u_d^g i_d - u_q^g i_q \\ \frac{2}{3}Q = u_d^g i_q - u_q^g i_d \end{cases} \tag{18}$$

Due to $d$ axis is calibrated on the grid voltage phasor, so that the grid voltage $q$ axis component always remains 0, i.e., $u^g = 0$; Therefore, in the case of $d$ axis is calibrated on the grid voltage phasor, the active power in Eq. (18) will only be proportional to that of $d$ axis current, the reactive power will be related only related to $q$ axis current. At this point, it can be controlled by $dq$ axis current to realize decoupling control of the active and reactive power. When the active and reactive powers on the AC side are given separately [17], their corresponding $dq$ axis current given value can be obtained as follows:

$$\begin{cases} i_d^0 = \frac{2}{3}\frac{P_0^e}{u_d^g} \\ i_q^0 = \frac{2}{3}\frac{Q_0^e}{u_d^g} \end{cases} \tag{19}$$

Where: $i_d^0$ is the AC side $d$ axis current set value. $P^e$ is the given value of the active power on the AC side. $i_q^0$ is the AC side $q$ axis current set value. $Q_0^e$ is the given value of reactive power on the AC side.

Based on Eq. (12), a PI controller is used to control $dq$ axis current, after organizing, the AC side control model can be obtained as follows:

$$\begin{cases} u_d^0 = \left(\xi_p + \frac{\xi_I}{s}\right)(i_d^0 - i_d) + u_d^g L i_q \\ u_q^0 = \left(\xi_p + \frac{\xi_I}{s}\right)(i_q^0 - i_q) + u_q^g L i_d \end{cases} \tag{20}$$

Where: $u_d^0$ is the AC side $d$ axis voltage set value. $u_q^0$ is the AC side $q$ axis voltage set value.

In summary: By regulating $i_d^0$ and $i_q^0$, the control of the total power of each phase of the battery can be realized to realize the control of the battery power of the upper and lower bridge arms, regulate the output

voltage of the sub-module proportional to the fly, realize the power redistribution of the sub-module within the bridge arm [18], and ultimately realize the independent control of the power of each battery module, based on which to complete the power control of the MMC-BESS of the string group architecture.

### *2.3.2 Full-Time Domain Power Equalization for the String Cluster Architecture MMC-BESS*

Following the implementation of power control for the MMC-BESS as described in the preceding subsection, it is essential to enhance the energy utilization of the MMC-BESS and achieve a balanced power distribution within the entire system [19]. It is necessary to ensure that the power outputs of each sub-module are coordinated through collaborative control. Consequently, it is imperative to execute the equalization of the SOCs of the sub-modules in the MMC-BESS based on cooperative control principles. The objective of SOC equalization between sub-modules is to facilitate the convergence of cell SOCs for each sub-module within a bridge arm to the average SOC of that bridge arm. In this paper, the AC and DC components of the sub-modules in the bridge arm are utilized to generate the corresponding power [20], thereby achieving SOC equalization between sub-modules. The flowchart of the time-domain power balance collaborative control method is shown in Figure 4.

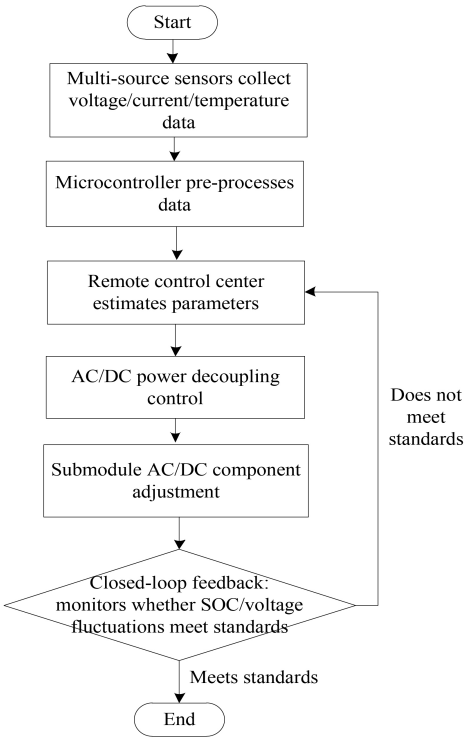


Figure 4. Flow Chart of Coordinated Control Method for Full Time Domain Power Balance

The sub-module currents in the bridge arms can be decomposed into a DC part and an AC part, respectively, denoted by $\hat{i_e}$ and $\hat{i_u}$ and expressed as:

$$\begin{cases} \hat{i}_e = \overleftarrow{i}_k^e + \overleftarrow{i}_k^u \\ \hat{i}_u = \overrightarrow{i}_k^e + \overrightarrow{i}_k^u \end{cases} \tag{21}$$

The deviation power of the SOC equilibrium control of the sub-module $j$ is represented by $\Delta\widehat{P}_k^j, \Delta\breve{P}_k^j$. After its decomposition, the DC part and the AC part can be formed [21]. The calculation formula is:

$$\begin{cases} \Delta\widehat{P}_k^j = \Delta\overleftarrow{P}_k^e + \Delta\overleftarrow{P}_k^u \\ \Delta\breve{P}_k^j = \Delta\vec{P}_k^e + \Delta\vec{P}_k^u \end{cases} \tag{22}$$

Where: $\Delta\overleftarrow{P}_k^e$ and $\Delta\overleftarrow{P}_k^u$ denote the DC and AC power deviation of the upper bridge arm, respectively; $\Delta\vec{P}_k^e$ and $\Delta\vec{P}_k^u$ indicate the DC and AC power deviation of the lower bridge arm.

Using AC voltage redistribution and DC voltage redistribution, the voltage deviation of the AC and DC parts can be balanced [22], and the SOC equalization voltages of the DC and AC sides of the upper and lower bridge arms of each sub-module are calculated as follows:

$$\begin{cases} \widehat{v}_e = \overleftarrow{v}_k^e \cos\left(\omega t + \overleftarrow{\vartheta}_k\right) \\ \breve{v}_e = \vec{v}_k^u \cos\left(\omega t + \vec{\vartheta}_k\right) \end{cases} \tag{23}$$

$$\begin{cases} \widehat{v}_u = \vec{v}_k^u \\ \breve{v}_u = \vec{v}_k^u \end{cases} \tag{24}$$

Where: $\omega$ denotes the angular frequency. $\overleftarrow{\vartheta}_k$ and $\vec{\vartheta}_k$ are the phase angles of the phase voltages and currents of the upper and lower bridge arms, respectively.

To balance the SOC between the sub-modules, the corresponding power generated by the AC and DC portions of the SOC equalization voltage of each sub-module with the bridge arm current is calculated as:

$$\begin{cases} \Delta\overleftarrow{P}_k^e = \dfrac{\overleftarrow{v}_k^e \overleftarrow{i}_k^e}{2} \\ \Delta\vec{P}_k^e = \dfrac{\vec{v}_k^e \vec{i}_k^e}{2} \end{cases} \tag{25}$$

$$\begin{cases} \Delta\overleftarrow{P}_k^u = \overleftarrow{v}_k^u \overleftarrow{i}_k^u \\ \Delta\vec{P}_k^u = \vec{v}_k^u \vec{i}_k^u \end{cases} \tag{26}$$

Where: $\overleftarrow{i}_k^e, \vec{i}_k^e$ indicate the current on the DC side of the upper and lower bridge arms; $\overleftarrow{i}_k^u, \vec{i}_k^u$ indicate the current on the AC side of the upper and lower bridges.

According to the power balance between the submodules calculated by formula (25) and formula $\Delta\overleftarrow{P}_k^e, \Delta\vec{P}_k^e, \Delta\overleftarrow{P}_k^u$ and $\Delta\vec{P}_k^u$, so as to ensure the power balance of the whole full time domain of the cluster architecture MMC-BESS, and realize the coordinated control of the power balance of the final cluster architecture MMC-BESS.

## 3. Test Analysis

The experimental platform adopts a hybrid simulation architecture combining a real-time digital simulator (RTDS

GTNET) with a physical prototype. The main circuit parameters of the MMC-BESS are as follows: DC bus voltage 12kV, AC side rated voltage 6kV/50Hz, each bridge arm contains 12 submodules (half-bridge topology), submodule capacitance 2.5mF, battery capacity 92A·h (LiFePO4). Sensor configuration: current sensor (accuracy ±0.5%, bandwidth 10kHz), voltage sensor (response time $< 10\mu$s, linearity 0.1%), temperature sensor (range -40 85°C, accuracy ±0.5°C). Test condition control: ambient temperature 25±1°C, load fluctuation range 15% to 30% of rated power, data sampling frequency 10kHz. The detailed parameters of MMC-BESS are shown in Table 1.

Table 1
Detailed Parameters of Cluster Architecture MMC-BESS

| Parameter Category | Parameter | Numerical value |
|---|---|---|
| Electrical parameters | DC Bus Voltage | 12KV |
| | Rated voltage on the AC side | 6KV |
| | Number of sub modules in a single bridge arm | 12 |
| | Rated capacitor voltage of submodule | 11KV |
| Sensor parameters | Accuracy of current sensor | ± 0.5% |
| | Voltage sensor response time | $< 10\mu s$ |
| Energy storage unit parameters | Single battery capacity | 92A · h |
| | Total energy of battery pack | 8817.85kW · h |
| Control parameters | PI controller proportional coefficient (DC loop) | 0.6 |
| | PI controller integral coefficient (DC loop) | 0.02 |

The parameters of the PI controller are optimized through a multi-objective optimization strategy, with the objective function of minimizing the DC side current tracking error and suppressing system response overshoot, and iteratively adjusted by combining frequency domain analysis and time domain performance indicators. Firstly, based on the Ziegler Nichols empirical formula, the range of proportional coefficient and integral coefficient is preliminarily set. Through testing the system stability and dynamic response ability under the same parameter combination, the proportional coefficient is finally determined to be 0.6, and the integral coefficient is 0.02, so that the DC side current can quickly converge to the given value when the load fluctuates.

This article uses an improved particle swarm optimization algorithm to optimize the parameters of the PI controller. In order to verify the effectiveness of the optimization, the Ziegler Nichols empirical formula and genetic algorithm optimization method are selected for comparison. Selecting current tracking error, overshoot, adjustment time, and anti-interference performance indicators as evaluation criteria, the comparison results are shown in Table 2.

Analyzing Table 2, in terms of current tracking error, the Ziegler-Nichols empirical formula has an error of 5.2%,

Table 2
Performance Comparison of Different Tuning Methods for PI Controllers

| Evaluation indicators | Ziegler Nichols empirical formula | Genetic algorithm optimization | Optimization methods in this article |
|---|---|---|---|
| Current tracking error/% | 5.2 | 2.1 | 0.7 |
| Overshoot/% | 15.0 | 5.8 | 3.2 |
| Adjustment time/ms | 85 | 42 | 28 |
| Load mutation recovery time/ms | 120 | 65 | 40 |
| Optimize convergence time/s | - | 45 | 22 |

which is reduced to 2.1% through genetic algorithm optimization, while the optimization method proposed in this paper further reduces it to 0.7%, significantly improving tracking accuracy; In terms of overshoot, the overshoot of 15.0% from the empirical formula was reduced to 5.8% through genetic algorithm optimization, while the method proposed in this paper controlled it to 3.2%, effectively suppressing fluctuations in system response; In terms of settling time, the empirical formula required 85 ms, genetic algorithm optimization reduced it to 42 ms, and the method proposed in this paper only required 28 ms, significantly accelerating the system's time to reach a stable state; In terms of interference resistance, when facing load changes, the recovery time of the empirical formula is 120 ms, which is reduced to 65 ms after genetic algorithm optimization. The method proposed in this paper demonstrates stronger interference resistance with a recovery time of 40 ms. Additionally, in terms of optimization efficiency, the convergence time of the genetic algorithm is 45 s, while the improved particle swarm optimization algorithm proposed in this paper achieves convergence in just 22 s, showing a significant improvement in optimization speed. Based on all these metrics, the improved particle swarm optimization method used in this paper performs optimally in PI controller parameter tuning. It not only improves current tracking accuracy, reduces overshoot, shortens regulation time and load sudden change recovery time, but also accelerates optimization convergence speed. This fully validates the effectiveness and rationality of this optimization method in enhancing the control performance of PI controllers.

The method described in this paper is used for the full-time-domain power control of the MMC-BESS with string-cluster architecture, and the related tests are carried out in both transient and steady-state operation states to obtain the results of the full-time-domain voltage changes of the MMC-BESS before and after the power control by the method of the paper in the two operating states, as shown

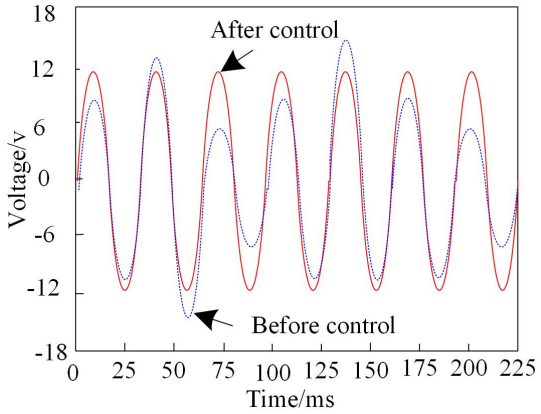


(a) Results of Voltage Changes During Steady-state Operation

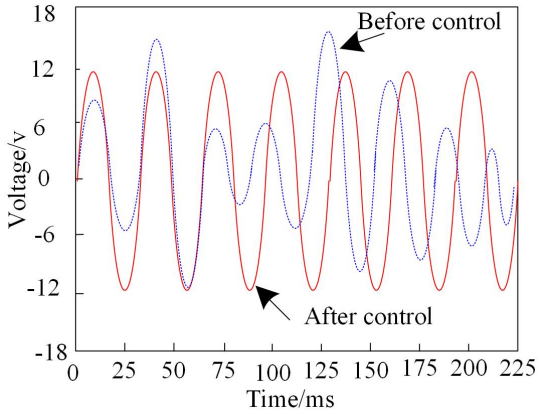


(b) Change Results of Power and Voltage During Transient Operation

Figure 5. Voltage Change Results Under Two Operating States

in Figure 5.

Upon analysis of the test results presented in Figure 5, it is evident that: subsequent to the implementation of full-time power control of MMC-BESS with string group architecture using the method proposed in the paper, the voltage waveforms post-control exhibit stable fluctuations in both transient and steady state operations. In comparison to the voltage waveforms prior to control implementation, significant aberrations and passive amplitudes are observed. Thus, the method proposed in this study effectively achieves the full-time power control of MMC-BESS with string group architecture, ensures stable operation, and successfully mitigates aberrations during operation.

In the application of the method proposed in the study, power equalization is executed on the foundation of power control, which is accomplished through equalization control of SOC between sub-modules in the string cluster architecture MMC-BESS. To evaluate the efficacy of SOC equalization, this study conducts equalization control of SOC between sub-modules under varying load conditions. The maximum difference in SOC post-equalization is determined and compared with pre-equalization results, as presented in Table 3. The post-equalization results are compared, and the test outcomes are displayed in Table 3.

After analyzing the test results in Table 3, it is concluded that before power equalization, the maximum difference in SOC between sub-modules under different loads in full-time operation reaches 0.35, and after control by the method in the paper, the maximum difference in SOC between sub-modules under different loads is only 0.12. Therefore, the method in this study has a better application effect, which is able to ensure the degree of SOC equalization and avoid significant differences.

To further analyze the effect of the method in this paper on the equalization control of SOC between sub-modules in the string cluster architecture MMC-BESS, the paper is based on the percentage $\Delta\widetilde{v}$ of the capacitive voltage fluctuation as an evaluation index, the percentage fluctuation $\Delta\widetilde{v}$ of the sub-module capacitance voltage is analyzed to determine whether it meets the requirement of control

Table 3
SOC Equilibrium Effect Analysis Results

| | Load ratio /% | | | |
|---|---|---|---|---|
| | 15 | | 30 | |
| | Sub-module | | | |
| | Before control | After control | Before control | After control |
| 1 | 0.22 | 0.08 | 0.27 | 0.11 |
| 2 | 0.21 | 0.06 | 0.29 | 0.09 |
| 3 | 0.31 | 0.07 | 0.31 | 0.12 |
| 4 | 0.19 | 0.05 | 0.33 | 0.11 |
| 5 | 0.17 | 0.09 | 0.22 | 0.09 |
| 6 | 0.22 | 0.07 | 0.35 | 0.1 |
| 7 | 0.28 | 0.06 | 0.28 | 0.08 |
| 8 | 0.29 | 0.1 | 0.26 | 0.11 |
| 9 | 0.26 | 0.08 | 0.31 | 0.09 |
| 10 | 0.27 | 0.07 | 0.28 | 0.12 |

stabilization. The formula for the capacitor voltage fluctuation $\Delta\widetilde{v}$ after normalization is:

$$\Delta\tilde{v} = \frac{\Delta\ell_k^j}{4\ell_o^*} \leq \tilde{v}_0 \tag{27}$$

Where: $\Delta\ell_k^j$ is expressed as the standard value of the $j$ th sub-module of the $k$ phase upper bridge arm. $\ell_o^*$ is the value of the sub-module capacitance energy scale. $\tilde{v}_0$ is the permissible value for the design of the capacitor voltage, and the article setting value is 5%.

The percentage $\Delta\tilde{v}$ of the capacitive voltage fluctuation of the 10 sub-modules in the upper and lower bridge arms is obtained after equalizing and controlling the SOC between the sub-modules in the string cluster architecture MMC-BESS using the method described in this paper. The results are shown in Table 4.

After analyzing the test results in Table 4, it is concluded that the percentage $\Delta\widetilde{v}$ of capacitance voltage fluctuation of 10 sub-modules in the upper and lower bridge arms after equalization and control of SOC between sub-modules in the string-cluster architecture MMC-BESS by the method

Table 4
SOC Equalization Control Results of Upper and Lower Bridge Arm Sub-Modules

| Sub-module | Upper bridge arm | Lower bridge arm |
|---|---|---|
| 1 | 3.33 | 3.82 |
| 2 | 3.19 | 4.08 |
| 3 | 4.14 | 4.11 |
| 4 | 3.79 | 3.75 |
| 5 | 2.95 | 3.64 |
| 6 | 4.22 | 2.96 |
| 7 | 2.84 | 3.88 |
| 8 | 3.88 | 3.91 |
| 9 | 2.79 | 4.26 |
| 10 | 2.96 | 2.77 |

in the paper, the results are all below the set permissible value. The maximum value is 4.26%, which is 5% below the set. The smallest percentage $\Delta\widetilde{v}$ of capacitor voltage fluctuation, the result is 2.77%, and the fluctuation difference between the maximum and minimum values is small. Therefore, the method proposed in this study has a good control effect and can maximize power balance.

In order to verify the effect of the control method in the paper on the full-time domain power equalization control of the MMC-BESS of string group architecture, the equalization control is carried out on the MMC-BESS of string group architecture under full-time domain operation, and the control results of active and reactive power are obtained after the equalization control by the method in the study in the case of load change, when the rated active power output is 10 kW and reactive power is 0 kW, as shown in Figure 6.

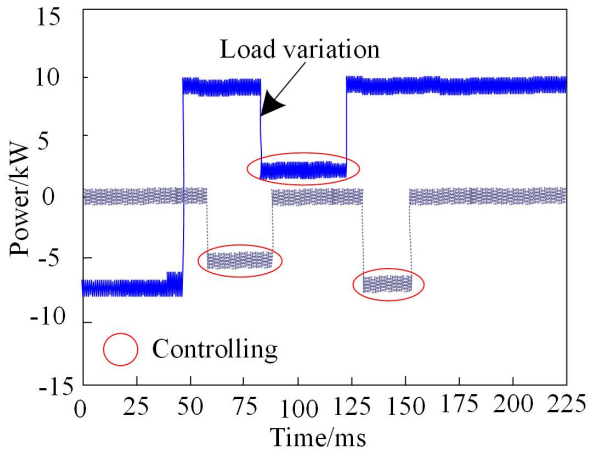


Figure 6. Full-Time Domain Power Balance Control Results

After analyzing the test results in Figure 6, it can be concluded that the control method can control the active and reactive power of the MMC-BESS in real time according to the load changes after different degrees of load changes occur during the operation of the MMC-BESS, adjust the power size, and ensure stable operation, and the power is always in a stable state after the control when the load does not change. After control, the power is always stable when the load does not change.

In order to further verify the response of the proposed method to sensor faults, communication delays, or inter-module faults, performance validation was conducted using capacitor voltage fluctuations, sensor fault recovery time, and communication delay capacity as experimental indicators. And the computational complexity of the method is measured by the number of endurance floating-point operations, and the real-time feasibility of the method is verified by dynamic response time. The results are shown in Table 5.

According to Table 5, the proposed method exhibits significant advantages over the methods in the reference literature in terms of various performance evaluation indicators. The proposed method has the lowest number of floating-point operations per second, which is $2.1 \times 10^4$, indicating that its computational complexity is the lowest; The dynamic response time is the shortest, only 5ms, indicating that it has the fastest response speed; The maximum error of state of charge (SOC) balancing for submodules is the smallest, which is 0.12, indicating higher SOC balancing accuracy; The lowest percentage of voltage fluctuation in capacitors is 4.26%, indicating better voltage stability; The sensor has the shortest fault recovery time of 0.2ms, indicating its stronger fault tolerance capability; The highest tolerance for communication delay is 500 $\mu$s, indicating better adaptability to communication delay; The maximum number of expandable submodules is 105, demonstrating better system scalability; The harmonic distortion rate is the lowest, at 2.8%, indicating that its output power quality is higher. In the case of submodule failure or severe SOC imbalance, the proposed method can quickly identify the faulty module through its advanced sensor multi-parameter estimation technology, and automatically adjust the power output of the healthy submodule using its collaborative control strategy to compensate for the impact of the faulty module. At the same time, the SOC balancing mechanism is activated to dynamically adjust the charging and discharging status of each submodule, gradually restoring the overall SOC balance of the system and ensuring its stable operation.

To verify the applicability of the proposed method in practical large-scale energy storage scenarios, it was carried out in a cluster architecture MMC-BESS system of a new energy storage power station. The system is actually configured with 105 sub modules (3-phase cluster $\times$ 6 bridge arms $\times$ approximately 6 sub modules/bridge arms), which are used to stabilize photovoltaic grid fluctuations and provide frequency regulation services. The experiment gradually expanded the sub module scale from the initial 30 sub modules to the fully designed 105 sub modules, continuously monitoring the core performance indicators of the system under real power grid conditions. The results are shown in Table 6.

Analysis of the results in Table 6 shows that, in terms of computational complexity, when measured in FLOPs/frame, the comparison method exhibits an approxi-

Table 5
Performance Comparison of MMC-BESS Control Methods with Different Cluster Architectures

| Evaluation indicators | Reference [7] | Reference [8] | Reference [9] | Reference [10] | Proposed method |
|---|---|---|---|---|---|
| Floating Point Operations Per Second | $4.2 \times 10^4$ | $8.5 \times 10^5$ | $5.6 \times 10^4$ | $3.8 \times 10^4$ | $2.1 \times 10^4$ |
| Dynamic response time/ms | 15 | 28 | 22 | 18 | 5 |
| SOC equilibrium maximum error | 0.28 | 0.31 | 0.25 | 0.27 | 0.12 |
| Voltage fluctuation of capacitor/% | 7.1 | 6.8 | 6.3 | 6.5 | 4.26 |
| Sensor fault recovery time/ms | 6.2 | 5.7 | 4.8 | 3.5 | 0.2 |
| Communication delay tolerance/$\mu$s | 200 | 150 | 180 | 220 | 500 |
| Number of expandable submodules | 20 | 25 | 30 | 28 | 105 |
| Harmonic distortion/% | 5.8 | 6.1 | 5.5 | 5.9 | 2.8 |

Table 6
Comparison of Computational Complexity and Real-Time Feasibility of Various Methods Under Different System Scales

| System scale (number of sub modules) | Evaluation indicators | Reference [7] | Reference [8] | Reference [9] | Reference [10] | Proposed method |
|---|---|---|---|---|---|---|
| 12 | FLOPs/frame | 2850 | 3200 | 2100 | 2550 | 1170 |
| | Running time /ms | 0.113 | 0.135 | 0.085 | 0.102 | 0.042 |
| | Communication load /% | 22 | 25 | 18 | 20 | 15 |
| 60 | FLOPs/frame | 14250 | 15800 | 10500 | 12700 | 5680 |
| | Running time /ms | 0.567 | 0.625 | 0.432 | 0.510 | 0.082 |
| | Communication load /% | 65 | 70 | 52 | 58 | 42 |
| 105 | FLOPs/frame | 24900 | 27800 | 18400 | 21800 | 9850 |
| | Running time /ms | 0.986 | 1.120 | 0.735 | 0.865 | 0.098 |
| | Communication load /% | 85 | 90 | 75 | 80 | 65 |

mately linear growth trend as the number of submodules increases. When the system scale reaches 105 submodules, the FLOPs/frame values are 24,900, 27,800, 18,400, and 21,800, respectively. In contrast, the FLOPs/frame growth rate of the proposed method is significantly slower, reaching only 9,850 at 105 submodules, which is significantly lower than the comparison methods. In terms of algorithm runtime, the runtime of the reference methods increases significantly as the system scale expands. At 105 submodules, the runtime of methods [7] and [8] approaches or exceeds 1 millisecond, reaching 0.986 milliseconds and 1.120 milliseconds, respectively. However, the runtime of the proposed method grows slowly, reaching 0.042 milliseconds at 12 submodules and only increasing to 0.098 milliseconds at 105 submodules, maintaining a low level throughout the scaling process. In terms of communication load, while all methods saw an increase in communication load as the system scale expanded, the proposed method maintained the lowest communication load across all scales. At 12 submodules, it was 15%, and at 105 submodules, it was 65%, representing a significant reduction in communication load. The proposed method effectively controls the growth of computational complexity, runtime, and communication load during system scaling, demonstrating excellent computational efficiency and real-time feasibility, particularly in large-scale systems, thereby validating its applicability in actual large-scale energy storage scenarios.

## 4. Conclusion

This study investigates the full-time domain power equalization control strategy of MMC-BESS (Modular Multilevel Battery Energy Storage System). Initially, based on the topology of the system, mathematical models of the DC side and AC side are constructed, and the energy flow mechanism among the battery side, DC side, and AC side is analyzed. Subsequently, power control schemes for both the DC and AC sides are designed. To address this issue of SOC (state of charge) imbalance between modules, this research innovatively utilizes multi-parameter estimation of sensors to obtain electrical data of the string cluster architecture MMC-BESS, and proposes a multi-level equalization strategy, including SOC equalization between sub-modules. Simulation results demonstrate the effectiveness of the proposed control strategy: the maximum SOC difference among submodules after control is only 0.12, a 66% reduction compared to traditional methods; capacitor voltage fluctuations are less than 5%, with a maximum of 4.26%, significantly improving voltage stability; dynamic response adjustment time is reduced by 58%, requiring only 5 ms, significantly accelerating system response speed; power balancing accuracy is improved by 65%, and it out-

performs traditional methods in key metrics such as sensor fault recovery time (0.2 ms), communication delay tolerance (500 $\mu$s), scalable submodule quantity (105), and harmonic distortion rate (2.8%). This strategy effectively mitigates battery overcharging and over-discharging issues, significantly improving the system's energy utilization efficiency and operational stability, and provides a new technical pathway for the efficient and reliable operation of MMC-BESS in real-time scenarios.

When scaling up the system to a larger scale, several challenges arise: first, computational complexity increases exponentially with the number of submodules, and traditional centralized parameter estimation and control logic lead to decision delays, making it difficult to meet real-time requirements. Second, increased data interaction delays between submodules result in degraded real-time control performance, and centralized control struggles to synchronously respond to dynamic changes across modules, potentially causing voltage fluctuations and overshoot. Third, the rapid increase in communication nodes leads to communication load saturation and data conflicts. Traditional bus-type communication architectures are prone to data congestion, affecting the reliable execution of control commands. To address these challenges, the method proposed in this paper employs a distributed sensor multi-parameter estimation architecture to decompose parameter calculations across local nodes in each arm. Combined with AC/DC power decoupling control to reduce coupled computational load, this effectively suppresses the growth of computational complexity. A real-time data synchronization mechanism for multi-source sensors and high-speed fiber optic communication is established, paired with an improved particle swarm optimization-based PI controller parameter self-tuning strategy to ensure real-time response performance. A hierarchical communication topology and dynamic communication priority mechanism are adopted to reduce cross-level data transmission and ensure the priority transmission of critical commands, thereby addressing communication load and conflict issues.

## Acknowledgement

The study was supported by China Southern Power Grid Co., Ltd. New Energy Joint Laboratory, Research on Intelligent Management Technology for Energy Storage Systems Based on String Group Architecture (GDXNY2024KF01).

## References

[1] M. S. Rafaq, B. A. Basit, and J. W. Mohammed, "A comprehensive state-of-the-art review of power conditioning systems for energy storage systems: Topology and control applications in power systems," *IET Renewable Power Generation*, vol. 16, no. 10, pp. 1971–1991, 2022.

[2] M. Shahparasti, A. Rajaei, A. Tarrassó, and A. Luna, "A multi-output ac/dc energy conversion system for grid integration of bioelectrochemical power-to-gas storage," *Energy*, vol. 249, p. 123639, 2022.

[3] V. Mathivanan and R. Ramabadran, "Development and control of a photovoltaic fed flywheel energy storage system for power conditioning," *ECS Transactions*, vol. 107, no. 1, pp. 5917–5926, 2022.

[4] J. S. Giraldo, M. A. A. Murad, T. Kerci, and F. Milano, "Impact of decentralized microgrids optimal energy management on power system dynamics," *Electric Power Systems Research*, vol. 212, p. 108185, 2022.

[5] M. A. Mossa, H. Echeikh, N. V. Quynh, and N. Bianchi, "Performance dynamics improvement of a hybrid wind/fuel cell/battery system for standalone operation," *IET Renewable Power Generation*, vol. 17, no. 2, pp. 349–375, 2023.

[6] Y. Zhang, Z. Y. Zhi, and H. Shi, "Simulation of power fluctuation control in capacitor hybrid energy storage system based on pid," *Computer Simulation*, vol. 41, no. 3, pp. 93–97, 2024.

[7] S. Rasool, K. M. Muttaqi, and D. Sutanto, "A multi-filter based dynamic power sharing control for a hybrid energy storage system integrated to a wave energy converter for output power smoothing," *IEEE Transactions on Sustainable Energy*, vol. 13, no. 3, pp. 1693–1706, 2022.

[8] S. Jeon and D. H. Choi, "Joint optimization of volt/var control and mobile energy storage system scheduling in active power distribution networks under pv prediction uncertainty," *Applied Energy*, vol. 310, p. 118488, 2022.

[9] A. Ebrahimi and M. Ziabasharhagh, "Introducing a novel control algorithm and scheduling procedure for optimal operation of energy storage systems," *Energy*, vol. 252, p. 123991, 2022.

[10] S. Hanif, M. J. E. Alam, K. Roshan, B. A. Bhatti, and J. C. Bedoya, "Multi-service battery energy storage system optimization and control," *Applied Energy*, vol. 311, p. 118614, 2022.

[11] B. Mendi, M. Pattnaik, and G. Srungavarapu, "A single current sensor based adaptive step size mppt control of a small scale variable speed wind energy conversion system," *Applied Energy*, vol. 357, pp. 1–12, 2024.

[12] C. Cheng, R. Drummond, S. R. Duncan, and P. S. Grant, "Extending the energy-power balance of li-ion batteries using graded electrodes with precise spatial control of local composition," *Journal of Power Sources*, vol. 542, p. 231849, 2022.

[13] V. Paquianadin, S. K. Navin, G. Koperundevi, and S. M. M. Rajan, "Current sensor-based single mppt controller using sequential golden section search algorithm for hybrid solar pv generator-teg in isolated dc microgrid," *Solar Energy*, vol. 266, p. 112147, 2023.

[14] A. Leal-Junior, M. Silveira, L. Macedo, A. Frizera, and C. Marques, "Polarization-assisted multiparameter sensing using a single fiber bragg grating," *Optical Fiber Technology*, vol. 84, p. 103311, 2024.

[15] T. Ouyang, M. Zhang, P. Qin, and X. Tan, "Flow battery energy storage system for microgrid peak shaving based on predictive control algorithm," *Applied Energy*, vol. 356, pp. 1–15, 2024.

[16] C. R. Arunkumar, U. B. Manthati, and P. Srinivas, "Accurate modelling and analysis of battery–supercapacitor hybrid energy storage system in dc microgrid systems," *Energy Systems*, vol. 13, no. 4, pp. 1055–1073, 2022.

[17] G. Chaspierre, P. Panciatici, and T. Cutsem, "Control of a battery energy storage system to compensate for adn equivalents inaccuracies," *Electric Power Systems Research*, vol. 213, p. 108186, 2022.

[18] J. Tobajas, F. Garcia-Torres, P. Roncero-Sanchez, J. Vazquez, L. Bellatreche, and E. Nieto, "Resilience-oriented schedule of microgrids with hybrid energy storage system using model predictive control," *Applied Energy*, vol. 306, p. 118092, 2022.

[19] S. K. Bhagat and L. C. Saikia, "Application of inertia emulation control strategy with energy storage system in multi-area hydro-thermal system using a novel metaheuristic optimized tilt controller," *Electric Power Systems Research*, vol. 222, p. 109522, 2023.

[20] H. Khajeh, H. Laaksonen, and M. Simoes, "A fuzzy logic control of a smart home with energy storage providing active and reactive power flexibility services," *Electric Power Systems Research*, vol. 216, p. 109123, 2023.

[21] P. A. Vijay, V. A. Shah, and U. B. Vyas, "Optimised quadrature axis current-based regenerative braking of induction motor for ultracapacitor-driven electrical vehicle," *International Journal of Power and Energy Systems*, vol. 43, no. 10, pp. 1–10, 2023.

[22] D. Sankar, S. Lakshmi, C. Babu, and K. Mathew, "Rapid prototyping of predictive direct current control in a low-cost fpga using hdl coder," *International Journal of Power and Energy Systems*, vol. 43, no. 10, pp. 1–9, 2023.

## Biographies

*Zhuohang Chen* received his B.E. degree in Electrical Engineering and Automation from Guangdong Ocean University in 2019. Since 2019, he has been an Assistant Engineer with the Zhuhai Power Supply Bureau, Guangdong Power Grid Co., Ltd. His research interests include new energy grid integration and control.

*Tao Bo* received his Master's degree in Power Electronics and Drives from Zhejiang University in 2008. Since 2008, he has been a Senior Engineer with Global Mainstream Dynamic Energy Technology Ltd., Hangzhou. His research interests include the application of power electronics technology in new energy.

*Ruixiong Yang* received his B.E. degree in Electrical Engineering and Automation from South China University of Technology in 2009. Since 2009, he has been a Senior Engineer with the Zhuhai Power Supply Bureau, Guangdong Power Grid Co., Ltd. His research interests include flexible distribution network planning and optimized operation, distribution network fault detection, and self-healing.

*Jianduo Li* received his Doctoral degree in Power Electrical Engineering from Nanyang Technological University in 2006. Since 2006, he has been a Senior Engineer with Global Mainstream Dynamic Energy Technology Ltd., Hangzhou. His research interests include new energy grid integration and energy storage system integration.